

1 Low Dose Ionizing Radiation Strongly Stimulates Insertional 2 Mutagenesis in a γ H2AX Dependent Manner

3
4
5
6 Alex N. Zelensky^{1,2*}, Mascha Schoonakker¹, Inger Brandsma¹, Marcel Tijsterman³,

7 Dik C. van Gent^{1,2}, Jeroen Essers^{1,4,5}, Roland Kanaar^{1,2*}

8
9
10
11 ¹Department of Molecular Genetics, ²Oncode Institute, Erasmus MC, PO Box 2040, 3000 CA,
12 Rotterdam, The Netherlands

13 ³Human Genetics, Leiden University Medical Center, PO Box 9600, 2300 RC, Leiden, The Netherlands

14 ⁴Department of Radiation Oncology, Erasmus MC, PO Box 2040, 3000 CA, Rotterdam, The
15 Netherlands

16 ⁵Department of Vascular Surgery, Erasmus MC, PO Box 2040, 3000 CA, Rotterdam, The Netherlands

17 * Corresponding authors: r.kanaar@erasmusmc.nl and a.zelensky@erasmusmc.nl

1 Abstract

2 Extrachromosomal DNA can integrate into the genome with no sequence specificity producing an
3 insertional mutation. This process, which is referred to as random integration (RI), requires a double
4 stranded break (DSB) in the genome. Inducing DSBs by various means, including ionizing radiation,
5 increases the frequency of integration. Here we report that non-lethal physiologically relevant doses
6 of ionizing radiation (10-100 mGy), which are within the range produced by medical imaging
7 equipment, stimulate RI of transfected and viral episomal DNA in human and mouse cells with an
8 extremely high efficiency of up to 10 fold. Genetic analysis of stimulated RI (S-RI) revealed that it is
9 distinct from the background RI, as it requires histone H2AX S139 phosphorylation (γ H2AX) and is not
10 reduced by DNA polymerase θ (*Pol θ*) inactivation. We further show that S-RI efficiency is not affected
11 by the disruption of the main DSB repair pathways (homologous recombination and non-homologous
12 end joining), and that double deficiency in MDC1 and 53BP1 phenocopies γ H2AX inactivation. The
13 robust responsiveness of S-RI to physiological amounts of DSBs has implications for radiation risk
14 assessment and can be exploited for extremely sensitive, macroscopic and direct detection of DSB-
15 induced mutations.

16 17 18 19 Keywords:

20 Random integration, extrachromosomal DNA, insertional mutagenesis, γ H2AX, DSB repair, low dose
21 irradiation.
22
23
24

1 Introduction

2 Extrachromosomal DNA – endogenous, viral or transfected – can integrate into the genomic DNA,
3 resulting in an insertional mutation. This type of mutagenesis has been primarily studied in the
4 context of exogenous DNA that enters the nucleus as a result of transfection or viral infection, and
5 has several important practical implications.¹ It is used to produce transgenic cell lines and organisms
6 for research and biotechnological applications. Random integration (RI) of transcription-blocking
7 constructs has been exploited as a form of untargeted but traceable mutagenesis (“gene trapping”).
8 Integration of exogenous DNA is an important factor in several therapeutic approaches, where it is
9 regarded as beneficial (stable restoration of a missing gene) or dangerous (insertion near an
10 oncogene and its activation). Viral integration into the genome has been considered as a contributing
11 factor in oncogenesis, even for viruses that do not encode an active integration function.² During
12 precise homology-driven modification of the genome (gene targeting), random integration of the
13 targeting construct is an unwanted side effect that severely limits the application of this powerful
14 technique in the vast majority of organisms.³

15 The presence of extrachromosomal DNA is a physiological condition, as a sizable pool of it exists in
16 the majority of normal cells in tissues, and includes fragments of nuclear and mitochondrial DNA
17 released due to damage repair, telomeric DNA circles,⁴ non-integrating viral genomes,⁵ mobile
18 genetic elements and phagocytized extracellular DNA.⁶ According to one estimate, the relative
19 fraction of such extrachromosomal DNA in normal tissues can be substantial, reaching 0.1-0.2% of
20 total DNA content,⁷ which is comparable to other major genomic components such as telomeres
21 (0.4%). How episomal DNA interacts with the genomic DNA and repair systems is not well
22 understood.

23 Insertion of exogenous DNA into a chromosome can be described by a simple and intuitive model as
24 mis-repair of a double strand break (DSB) in the genomic DNA by non-homologous end joining that
25 traps an extrachromosomal DNA fragment happening to be in the vicinity of the DSB.^{8,9} This model
26 predicts that the proximity of an ongoing DSB repair event to an extrachromosomal DNA molecule
27 will determine the frequency of the insertion, and therefore that increasing the frequency of DSBs
28 above background by inflicting additional damage will increase the likelihood of integration. This
29 prediction has been confirmed numerous times in various cell lines and with different DNA vectors
30 using doses of > 0.5 Gy of ionizing radiation (γ - and X-rays), which is arguably the best-studied method
31 of DSB induction.¹⁰⁻²³ RI stimulation by DSB-inducing chemicals and enzymes has also been
32 demonstrated, as well as some non-DSB inducing genotoxic agents.^{16,21,24-35} In the latter case the
33 stimulation can be explained by indirect DSB induction during replication.

34 Genomic integration of extrachromosomal DNA is referred to in the existing literature as RI,
35 illegitimate recombination, illegitimate integration, stable integration, stable transformation, non-
36 homologous integration or insertional mutation.⁸ Although it is not perfect, we chose to use the first

1 term. In the context of RI stimulated by DNA lesions we use the term stimulated RI (S-RI). Here we
2 report the following, and to our knowledge so far unidentified, properties of the S-RI phenomenon.
3 Firstly, we found that extremely low doses (10-50 mGy), similar to those encountered during routine
4 medical diagnostic procedures, strongly stimulate the integration of transfected DNA and episomal
5 viral DNA. Secondly, a screen of multiple knock-out mouse embryonic stem (ES) cell lines revealed
6 that contrary to expectation, disruption of the two major DSB repair pathways has no effect on S-RI,
7 and thirdly we showed that phosphorylation of H2AX on serine 139 and recruitment of the adaptor
8 protein MDC1, involved in DNA damage response, are essential for the process.

10 Results

11 Integration is strongly stimulated by physiologically relevant doses of radiation

12 To investigate the effect of low dose irradiation (< 1 Gy) on RI we transfected ES cells by
13 electroporation with circular or linearized plasmid DNA containing a puromycin resistance gene,
14 divided the cells equally over several culture dishes, and irradiated the dishes using ¹³⁷Cs γ -irradiation
15 source with a set of doses ranging from 0.01 to 1 Gy [Fig 1A,B]. Remarkably, even the lowest dose
16 tested already led to an increase in the number of puromycin-resistant colonies formed after 6-8 days
17 of selection [Fig 1B], with a 7.5 ± 0.8 -fold increase at a dose of 200 mGy. The response was linear
18 between 10 and 200 mGy, then plateaued between 200 and 500 mGy, and decreased at 1 Gy.

19 The sensitivity of the response to the extremely low doses, the plateauing dose response, and the
20 high magnitude of the stimulation (up to 10-fold) distinguish our findings from numerous previous
21 reports of the phenomenon, as they generally studied doses above 1 Gy.^{12-19,22} It is remarkable that
22 the exquisite sensitivity of the assay to physiologically relevant amounts of induced DNA damage
23 appears to have escaped experimental scrutiny for more than half a century. Intrigued by this, we
24 went on to verify the generality of the S-RI phenomenon using different DSB induction methods, cell
25 lines, DNA vectors and assay endpoints. The lower end of the dose range we tested overlaps the dose
26 range of certain medical imaging procedures (e.g. 1-30 mGy for computed tomography (CT) and
27 fluoroscopy²⁴). We scanned freshly transfected ES cell suspension in a micro-CT instrument (Quantum
28 FX, PerkinElmer) used for mouse imaging. One to five sequential scans were performed at the lowest
29 resolution, each scan delivering 13 mGy based on the manufacturer's data. A single scan produced a
30 clear increase in integration frequency (2.28 ± 0.17 , $n=7$) and consecutive scans resulted in a dose
31 response curve similar to what we observed with the ¹³⁷Cs source [Fig 1C]. Human HeLa cells
32 transfected with the plasmid DNA by electroporation or lipofection performed similarly to mES cells in
33 the S-RI colony formation assay [Fig S1A,B].

34 To confirm that our observations were not limited to plasmid DNA transfection or antibiotic selection,
35 we performed S-RI experiments using non-replicating episomal viral vectors and with fluorescent

1 marker detection by FACS. Recombinant adeno-associated virus type 2 (rAAV2) has a single-stranded
2 DNA genome, and while it can integrate in cultured human cells with some sequence specificity
3 conferred by the *rep* protein, wild-type AAV2 infecting human tissues and *rep*-deleted rAAV2 vectors
4 persist as episomes and integrate infrequently and with no detectable specificity.^{5,25} We added
5 lysates containing rAAV2 particles encoding GFP to the HeLa cell culture media, incubated overnight
6 to allow infection to occur, re-seeded the cells into a series of dishes and irradiated them with 0.02-1
7 Gy. The fraction of cells expressing GFP was ~60% two days after the infection and gradually
8 decreased over time due to dilution and loss of rAAV2-GFP episomes in dividing cells. At day 13 only
9 0.05-0.1% of unirradiated cells remained GFP-positive, presumably due to stable integration.²⁶ The
10 GFP-positive fraction increased linearly with the dose in irradiated cells [Fig 1D, S1C]. Transfection of
11 human U2OS cells with plasmid DNA containing a GFP minigene, followed by FACS 14-21 days later,
12 further confirmed that selection is not required to observe the S-RI effect [Fig S1D]. We also observed
13 S-RI [Fig 1E] with integrase-deficient HIV-1 lentiviral (IDLV) vectors^{27,28} whose RNA genomes are
14 reverse-transcribed normally, but accumulate as circular or linear episomal DNA because of the
15 inactivating D64V mutation in the integrase.²⁹

16 Both IDLV and rAAV vectors were used previously to detect nuclease-induced DSBs.^{26,30,31} To show
17 that transfected plasmid DNA also integrates at the DSBs we used the DiVA-AID cell line, which allows
18 precise control over nuclear localization and degradation of the AsiSI nuclease that has hundreds of
19 recognition sites in human genome.³² We added 4-hydroxytamoxifen to induce AsiSI breaks
20 immediately after the transfection of plasmid DNA, and controlled the DSB dose by inducing AsiSI
21 degradation by adding auxin to the media 1 or 4 hours later [Fig 1F]. The dose-dependent increase in
22 the number of colonies we observed was consistent with the results we obtained using ionizing
23 radiation.

24 To better characterize the parameters affecting S-RI we studied its dependence on the timing of
25 irradiation and on the amount of transfected DNA. The stimulatory effect of irradiation dropped
26 precipitously shortly after transfection, but was still observed as late as 24 hours later when circular
27 plasmid DNA was used [Fig S1E,F]. We also performed an experiment in which the order of
28 transfection and irradiation was reversed, and still observed a stimulatory effect [Fig S1G]. This
29 demonstrates that S-RI is caused by the effect of IR on the host cell rather than on the transfected
30 DNA, further supporting the notion that the stimulation is achieved by DSB induction in the genomic
31 DNA. By modifying the amount of DNA electroporated into mES cells we revealed a striking and
32 opposing effects on S-RI and background RI [Fig 1G, S1H,I]. When DNA amounts were low (2 µg), S-RI
33 was very efficient, and background RI was low, while when high amount of DNA was electroporated
34 (100 µg), S-RI became inefficient, and background RI increased.

1 S-RI requires γ H2AX but not HR or NHEJ

2 A simple explanation to S-RI is that radiation creates DSBs into which transfected DNA can be ligated.
3 This model predicts that cells in which major DSB repair mechanisms, such as homologous
4 recombination (HR) and non-homologous end joining (NHEJ), are disrupted, will be more responsive
5 to S-RI, unless the repair deficiency negatively affects the enzymes involved in integration itself. We
6 performed the S-RI assay in mES cell lines where key DNA damage repair and response genes were
7 genetically inactivated. Surprisingly, we observed wild-type dose response curves in *Rad54*^{-/-} ES cells,
8 which have an HR deficiency phenotype,³³ and in *p53*^{-/-} cells lacking key DNA damage signaling
9 mediator, while in *DNA-PKcs*^{-/-} (*Prkdc*^{-/-}) cells deficient in a canonical NHEJ enzyme³⁴ a small reduction
10 in S-RI was observed [Fig 2A]. We recently demonstrated that in mES cells DNA polymerase θ is
11 responsible for the majority of background RI,³⁵ and canonical NHEJ proteins Ku70, Ku80 and LigIV
12 become important in the absence of Pol θ ; and similar observations were reported in human cells.³⁶
13 Surprisingly, S-RI was increased rather than suppressed in the Pol θ -deficient cells (*Polq*^{-/-}), and in the
14 Ku mutants [Fig 2B], which suggests that S-RI and background RI have distinct genetic dependencies.
15 In sharp contrast, cells deficient for H2AX,^{37,38} a histone variant whose post-translational
16 modifications are central to DNA damage response signaling, were near-completely immune to RI
17 stimulation by irradiation [Fig 2A]. This was difficult to reconcile with the previously described
18 phenotypes of *H2ax*^{-/-} cells, which are prone to translocations^{39,40} suggesting increased frequency of
19 DSBs in the absence of a major NHEJ defect. Background RI was normal in *H2ax*^{-/-} lines [Fig S2A],
20 further indicating that RI and S-RI are genetically distinct processes.

21 The S-RI defect was observed in two different *H2ax*^{-/-} cell lines and could be reverted by inserting a
22 wild-type copy of *H2ax* into the *Rosa26* “safe harbor” locus [Fig 2C, S2B,C]. We also tested variants of
23 H2AX with mutations in residues that are phosphorylated (S139) or ubiquitinated (K13, K15, K118,
24 K119) during DNA damage response signaling,⁴¹⁻⁴³ as well as Y142 required for interaction with the
25 key downstream effector MDC1.⁴⁴ Mutations in the lysines – these residues are common to all H2A
26 variants – did not impair S-RI, while S139A and Y142A mutants were indistinguishable from
27 uncomplemented *H2ax*^{-/-} cells [Fig 2C].

28 To determine if S-RI was permanently blocked or just stunted by *H2ax* inactivation we performed a
29 broad-dose S-RI experiment [Fig 2D], using doses up to 3 Gy. The gradual increase in S-RI efficiency
30 we observed in *H2ax*^{-/-} cells in this dose range indicated that the end joining reaction responsible for
31 the ligation of extrachromosomal DNA into the IR-induced DSB was inherently functional, but less
32 efficient in the absence of H2AX.

33 Finally, we wondered, which of the checkpoint kinases⁴⁵ phosphorylating H2AX at the sites of DNA
34 damage is involved in S-RI. Therefore, we performed experiments in the presence of chemical
35 inhibitors: KU-55933 specific for ATM,⁴⁶ VE-821 specific for ATR,⁴⁷ wortmannin that has highest
36 specificity for DNA-PKcs,⁴⁸ and UCN-01 for Chk1⁴⁹ at the concentrations we previously found to be

1 effective in mouse ES cells.⁵⁰ We also tested the effect of caffeine, which is widely used as a broadly
2 specific ATM/ATR/DNA-PKcs inhibitor, but which we found to lack this activity in ES cells, and to
3 strongly suppress gene targeting by HR.⁵⁰⁻⁵² Inhibition of ATM and ATR reduced S-RI efficiency [Fig
4 S2D], and the combination of the two inhibitors had an additive effect, which was even more
5 pronounced in *DnaPKcs*^{-/-} cells [Fig S2D]. In contrast UCN-01, caffeine and wortmannin had no effect
6 on S-RI. Taken together these results indicate that S-RI is dependent on phosphorylation of H2AX by
7 one of the partially redundant DNA damage response kinases.

8 Role of γ H2AX-Binding Proteins

9 Three proteins have been shown to directly bind H2AX in phospho-S139 dependent manner: MDC1,⁴⁴
10 53BP1⁵³ and MCPH1.⁵⁴ We engineered a series of mES knock-out cell lines [Fig 3, S3-S5] to test if S-RI
11 deficiency in cells that cannot form γ H2AX is due to the failed recruitment of these proteins. Based on
12 its role in promoting DSB repair via NHEJ over HR, 53BP1 would be a good candidate for the role of
13 the downstream effector, however neither the knock-out nor shRNA knock-down of 53BP1 affected
14 S-RI or background RI [Fig 3A, S3A,B, S4]. The most pronounced phenotype of MDC1-deficient cells
15 was a significant reduction in background RI, similar in magnitude to what we reported previously for
16 Pol θ .³⁵ However, unlike in Pol θ -deficient cells [Fig 2B], S-RI was partially suppressed in *Mdc1*^{-/-} cells
17 [Fig 3A], and reduced even further in the double *Mdc1*^{-/-}*53bp1*^{-/-} knock-out line. Inactivation of *Mdc1*
18 in *H2ax*^{-/-} cells did not further suppress S-RI, consistent with the downstream role of MDC1 in γ H2AX
19 signaling. *Mcph1* knock-out cells behaved like wild-type in the S-RI assay, but had elevated
20 background RI. The *Mcph1* mutation also reverted the partial suppression of S-RI by *Mdc1*
21 inactivation, as *Mdc1*^{-/-}*Mcph1*^{-/-} double mutant showed the same S-RI efficiency as wild-type cells.
22 Since we established that MDC1 contributes to both RI and S-RI efficiency, the positive effect of
23 MCPH1 deletion can be explained by its competition with MDC1 for phospho-S139 binding.

24 Discussion

25 We used a simple assay to re-examine a phenomenon known since the early days of research on
26 cultured eukaryotic cells.^{22,23} This makes a number of unexpected observations regarding radiation-
27 stimulated integration of extrachromosomal DNA we present here all the more interesting. The most
28 important of them are: high sensitivity to very low, physiologically relevant doses of irradiation, non-
29 linear dose dependence, independence of the best known DSB repair pathways, NHEJ and HR,
30 requirement of γ H2AX for stimulated but not background RI, and the complex involvement of γ H2AX-
31 interacting proteins.

32 Despite numerous reports describing the stimulation of RI by ionizing radiation, to our knowledge our
33 study for the first time reports the effects of doses <0.5 Gy, and in particular the striking dose-
34 dependent stimulation in the range 0.01-0.2 Gy. Previous studies performed with a dose range of 1-
35 10 Gy with different vertebrate cell lines, vectors and transfection methods, observed linear dose

1 dependence of stable colony numbers after adjustment for IR-induced reduction in
2 survival.^{12,15,18,19,22,23} Explanation of the dose-response curve plateauing we observed in the majority
3 of experimental systems we used [Fig 1, S1], and seen in some previous studies,^{14,17} requires a model
4 that considers more than just chromosomal DSBs as the factor limiting extrachromosomal DNA
5 integration. What can be the other bottleneck(s)? Transfection efficiency is clearly not one, as the
6 frequency of stable integration events (10^{-2} - 10^{-4}) is orders of magnitude lower than the number of
7 transfected cells ($>10^1$). Furthermore, we observed that decreasing the amount of transfected DNA
8 makes S-RI *more* efficient. The nature of the barrier limiting S-RI, which may be cell-intrinsic (e.g.
9 capacity of a DNA-binding protein, signals triggered by DSBs or transfected DNA above a certain
10 threshold), or reflect heterogeneity in the cell population, remains to be determined.

11 γ H2AX as a central factor involved in stimulated random integration

12 We observed a striking and unanticipated difference in S-RI between the wild-type and the *H2ax*^{-/-} ES
13 cells. Although γ H2AX is a widely used DNA damage marker and actively studied as such (reviewed in
14 ref. 55), the effects of H2AX deficiency on cells and organisms are generally described as “moderate”
15 or “mild”.^{37,38,56-59} The near-absolute dependence of S-RI on γ H2AX is among the most striking H2AX
16 phenotypes discovered to date. Several ways a DNA repair protein may affect RI can be envisaged: by
17 direct involvement in the NHEJ reaction, indirectly by influencing DSB repair pathway choice or
18 facilitating NHEJ protein recruitment etc., or by changing DSB persistence (longer half-lives due to
19 inefficient repair will increase the probability of encounter between a genomic DSB and an
20 extrachromosomal DNA molecule). Other indirect effects through chromatin mobility or packing
21 (accessibility) can also be considered.

22 H2AX contributes to efficient repair of DSBs by NHEJ. H2AX-deficient cells have increased frequency
23 of both background and induced chromosomal aberrations.^{37,38,58} V(D)J recombination although
24 superficially normal in *H2ax*^{-/-} mice^{37,38} has hidden alterations revealed by additional inactivation of
25 p53, Artemis or XLF.⁵⁵ On the other hand, sensitivity of H2AX-deficient cells to ionizing radiation
26 ranges from moderate³⁷ to marginally detectable,⁵⁸ and is always lower than core NHEJ mutants.³⁷
27 Moreover, some of this increased sensitivity can be attributed to impaired HR^{38,58,60,61} and a
28 compromised G2/M DNA damage checkpoint.^{58,62} Assays monitoring mutagenic repair of nuclease-
29 induced DSBs in a chromosomal reporter revealed no effect of H2AX deletion.⁶³ Data on DSB
30 clearance kinetics in H2AX-deficient cells is conflicting (refs 38,56 vs 64). Thus, previously described
31 involvement of H2AX in NHEJ does not provide a compelling explanation to S-RI suppression.

32 Among γ H2AX-binding proteins 53BP1 was a prime candidate for the role of the γ H2AX-dependent S-
33 RI mediator,^{65,66} as its retention at DSBs is γ H2AX-dependent,⁵⁹ it promotes DSB repair by NHEJ over
34 HR,⁶⁷ facilitates of the synapsis between distal DSBs⁶⁸ and increases the mobility of a chromosomal
35 DSBs.⁶⁹ However, we could only observe the effect of 53BP1 deletion on S-RI when MDC1 was also
36 absent. Moreover, we found that MDC1 rather than 53BP1 contributes to background RI, which was

1 also observed previously in human cells,^{44,70} and deletion of 53BP1 had no significant effect even
2 when combined with *Mdc1* inactivation. While several studies showed that 53BP1 recruitment to
3 ionizing radiation-induced foci is controlled by MDC1,⁷¹⁻⁷³ our results suggest an MDC1-independent
4 role of 53BP1, as double mutation *Mdc1*^{-/-}*53bp1*^{-/-} is required to recapitulate the effect of H2AX
5 deficiency on S-RI.

6 Are S-RI and RI distinct processes?

7 The S-RI and background RI have distinct genetic dependencies: while γ H2AX is required for S-RI, its
8 loss does not affect background RI; Pol θ has an opposite effect: it is responsible for the majority of
9 background RI events, but its deletion does not impair S-RI; Inactivation of *Mdc1* severely impairs
10 background RI,^{44,70} but has a much smaller effect on S-RI; *Mcp1* knock-out increases RI efficiency, but
11 has no effect on S-RI unless *Mdc1* is also inactivated. These observations can be interpreted as an
12 indication that S-RI and RI are mechanistically different. However, the models based on this
13 supposition and accommodating the observation we present here and previously³⁵ are inevitably
14 complex [Fig S3C], and require some uncomfortable assumptions. For example, we found that two
15 out of three γ H2AX-binding proteins we studied affect background RI (MDC1 stimulates, MCPH1
16 suppresses [Fig S3B]). If we postulate that background RI itself is γ H2AX-independent, we need to
17 conclude that each of the two proteins is coincidentally recruited in some γ H2AX-independent
18 manner.

19 The alternative is to suppose that at least some of the apparent genetic distinctions between RI and S-
20 RI are misleading, or that they stem from the factors that are beyond the simple “[DSB] • [ecDNA] →
21 end joining → insertion” model. As an example of the former, the concentration of background DSBs
22 in the *H2ax*^{-/-} cells (known to be genetically unstable), could be so high as to reach the saturation state
23 that is responsible for the plateauing of the dose-response curve. However, our broad-dose
24 experiment argues against this explanation [Fig 2D]. Factors outside of the DSB repair paradigm may
25 include alteration of the cellular state due to DNA damage and antiviral defense checkpoint
26 inductions we alluded to in the discussion of the dose-response plateau, role of H2AX and its
27 interactors in transport, chromatinization, persistence and integrity of the ecDNA, etc. Further genetic
28 exploration of the RI and S-RI phenomena should provide important clues. It is particularly interesting
29 to trace the connection between the upstream signaling proteins (H2AX, MDC1) and the end-joining
30 proteins responsible for the insertion reaction (Pol θ and canonical NHEJ).

31 Implications

32 Our results have several important implications. If the robust stimulation of insertional mutagenesis
33 by the doses well below what is currently considered harmful is not limited to cultured cells, it will be
34 important to consider elevated episomal DNA concentration – for example from viral infection – as a
35 confounding factor in assessing the risks of low dose irradiation. The S-RI assay is macroscopic and

1 thus simpler than direct and surrogate mutagenesis assays and damage detection methods (DNA
2 damage response foci counting), and is as sensitive as the alternatives. A high throughput version of it
3 can be developed for determining chemical genotoxicity at physiologically relevant concentrations. It
4 should be stressed that the assay detects irreversible mutagenic events rather than damage that may
5 or may not be repaired.

6 Analysis of the genetic dependencies of S-R1 revealed several unexpected findings, and demonstrated
7 that it provides tools to study functional interactions between the components of the convoluted
8 γ H2AX signaling pathway, NHEJ and other DSB repair proteins.

9 Methods

10 Cell lines

11 IB10 mouse ES cells, a clonal isolate of the E14 line,⁷⁴ and other mouse ES cell lines used in the study
12 were maintained on gelatinized plastic dishes as described.⁵⁰ ES cells were grown in 1:1 mixture of
13 DMEM (Lonza BioWhittaker Cat. BE12-604F/U1, with Ultraglutamine 1, 4.5 g/l Glucose) and BRL-
14 conditioned DMEM, supplemented with 1000 U/ml leukemia inhibitory factor, 10% FCS, 1x NEAA, 200
15 U/ml penicillin, 200 μ g/ml streptomycin, 89 μ M β -mercaptoethanol. *H2ax*^{-/-} (A) and (N) ES cells were
16 kindly provided by the Alt and Nussenzweig laboratories, respectively.^{37,38} HeLa and U2OS cells were
17 grown in DMEM, 10% FCS, 200 U/ml penicillin, 200 μ g/ml streptomycin. AID-AsiSI-ER U2OS cells were
18 a kind gift of Gaëlle Legube.³² HEK293T cells were grown in DMEM, 5% FCS, 200 U/ml penicillin, 200
19 μ g/ml streptomycin.

20 Generation of knock-out ES cell lines with CRISPR/Cas9

21 *Mdc1*, *Mcph1*, *53bp1* knock-out ES cells were produced by CRISPR/Cas9 stimulated gene targeting
22 with plasmid donor [Fig S4-S5]. The CRISPR/Cas9 expression plasmid (derived from pX459⁷⁵)
23 contained one or two sgRNA expression cassettes. Target sequences were (PAM underlined): for
24 *Mdc1* #2 AAGGTAGAGGGGAAATCTGAGG and #3 AACAGTAGTTCAGAAAGGTGGG within exons 3
25 and 4; for *53bp1* #1 TAGTTGAGGTCGGCTTGAGGTG upstream of the promoter and #2
26 CCATCAGTCAGGTCATTGAACCGG within exon 4; for *Mcph1* promoter targeting #1
27 CCGGCGCTTAAGGCGACGAAAGG and #2 AAAGCAACTTGAGGATATGGGGG, for *Mcph1* exon 4-5 #3
28 TGTTCATCGGTATTCAGTGCAGG and #4 TGTGCCTGACAGCTACAGGGAGG. Donor constructs contained
29 PGK-hyrgo (*Mdc1*) or PGK-neo (*Mcph1*, *53bp1*) selection cassettes. *Mdc1*^{-/-}*53bp1*^{-/-} and *Mdc1*^{-/-}*Mcph1*^{-/-}
30 ^{-/-} cells were produced from the *Mdc1*^{-/-} cell line. For each genotype two to four independent clones
31 were used in experiments.

32 For H2ax complementation NotI-linearized *Rosa26*⁷⁶ targeting vectors containing the human H2AX
33 CDS under the *H2ax* promoter and with *H2ax* 3'UTR were electroporated into $\sim 1-2 \times 10^7$ *H2ax*^{-/-}(N) ES
34 cells. The vectors were derived from *Rosa26* gene targeting vector pHA416 (a kind gift from Hein te

1 Riele) containing *Salmonella typhimurium* hisD coding sequence. Two days after electroporation
2 selection with 2 or 4 mM L-histidinol (Sigma, H6647) was started. Media was replaced every 2-4 days
3 for 10-14 days; colonies were picked and expanded. Single copy integration into the *Rosa26* locus was
4 confirmed by DNA hybridization on BamHI-digested genomic DNA with a 5' probe (PstI-Sall fragment,
5 from pHA607⁷⁷). H2AX expression was verified by immunoblotting with anti- γ H2AX (Millipore mouse
6 mAb clone JBW301) or anti-total H2AX antibody (Cell Signaling rabbit polyclonal #2595).

7 Constructs

8 Constructs used in this study were generated by homology-based cloning methods: SLIC,⁷⁸ In-Fusion
9 (Clontech), isothermal Gibson assembly⁷⁹ or recombineering with mobile reagents.⁸⁰ Pfx50
10 polymerase (Invitrogen) was used for PCR amplification of the construction elements in most cases,
11 Phusion (Finnzymes) or Platinum Taq (Invitrogen) polymerase were used to amplify from genomic
12 DNA or cDNA. Constructs were partially sequenced to verify the ligation junctions and ensure the
13 absence of PCR-induced mutations. Maps and details are available upon request. List of
14 oligonucleotides and constructs is provided in Supplementary data file 1.

15 pLPL, the construct used in the majority of S-RI experiments, was derived from the construct loxP-
16 PGK-gb2-neo-polyA-loxP cassette in pGEM-T Easy originally designed to engineer knock-out alleles
17 using recombineering (Francis Stewart lab, distributed at 2007 EuTRACC workshop on
18 recombineering), referred to as pLNL. A dual (bacterial (gb2) and eukaryotic (PGK)) promoter drives
19 the antibiotic resistance gene allowing selection in both hosts. Neomycin phosphotransferase (*neo*)
20 was replaced with puromycin N-acetyltransferase (*pac*, puro) or hygromycin phosphotransferase
21 (*hygro*) using recombineering to produce pLPL and pLHL, respectively. For linearization pLPL was
22 digested with DraI, phenol-extracted, precipitated with isopropanol and dissolved in deionized water.

23 *H2ax* complementation constructs used to insert a single copy of the human or mouse *H2AX* CDS
24 under native mouse *H2ax* promoter and 3'UTR were engineered by replacing the backbone and
25 removing the PGK-polyA cassette from the pHA416 vector (a gift from Hein te Riele) to create a
26 unique XhoI site between the histidinol trap cassette and the 3' homology arm (pAZ025). A 1721-bp
27 fragment of the mouse *H2ax* locus was PCR-amplified using H2AXwhole-F/-R primers first into a
28 shuttle vector, and then re-cloned into pAZ025, resulting in pAZ026. Analogous constructs were
29 engineered with human H2AX and its mutants by PCR amplification of the promoter and UTR regions
30 from pAZ026 and coding sequences from the corresponding pMSCVpuro constructs⁴³ (pAZ080-
31 pAZ085); Y142A mutation was added by site-directed mutagenesis (pAZ122).

32 S-RI assays

33 Drug resistant colony formation was used as a measure of stable RI frequency in the majority of
34 experiments. In a typical experiment 6×10^6 mouse ES cells were electroporated in 450 μ l growth
35 media with 10 μ g circular or linearized pLPL (puro) or pAZ095 (GFP, puro) plasmid DNA using

1 GenePulser Xcell apparatus (118 V, 1200 μ F, ∞ Ω , exponential decay). pEGFP-N1 plasmid (10 μ g) was
2 co-electroporated with pLPL to estimate transfection efficiency in the experiments, where absolute
3 targeting efficiency was determined. In the initial experiments electroporated cells were re-
4 suspended in 37-68 ml growth media; the suspension was distributed over 5-8 10 cm dishes at 7 ml
5 per dish. In later experiments, involving larger number of cell lines, electroporated cells were re-
6 suspended in media and equally distributed into 1.5 ml microcentrifuge or 0.2 ml PCR tubes at 0.1-1
7 ml per tube. Cells were irradiated within 1 hr after seeding with different doses using 137 Cs source
8 (Gammacell) or X-ray apparatus (RS320, Xstrahl). A metal attenuator reducing the dose rate by ~50%
9 was used to deliver doses <100 mGy in low-dose irradiation experiments with Cs source. For micro-CT
10 irradiation cells in 6 cm culture dishes or in 1.5 ml microcentrifuge tubes were scanned (Quantum FX,
11 Perkin Elmer) in the low resolution mode (73 mm f.o.v., 17 sec, 148 mm pixel size), repeatedly 1-5
12 times. The initial number of cells used for electroporation was increased to compensate for low
13 plating efficiency of some knock-out cell-lines (e.g. *H2ax*^{-/-} and their derivatives). After irradiation in
14 microtubes cells were plated in 10 ml media in 10 cm dishes. To estimate plating efficiency at various
15 irradiation doses 2-4 μ l aliquots of irradiated cell suspension was plated into 6-well plates in
16 triplicates. Puromycin (1.5 μ g/ml) selection was started one day after electroporation; media was
17 changed as required until macroscopically visible colonies were formed. Colonies were washed with
18 PBS, stained with Coomassie Brilliant Blue (100 mg/l in 40% methanol, 10% acetic acid), and counted
19 directly or after photographing. Colony counts were adjusted for transfection and plating efficiencies.
20 RI stimulation was determined by dividing the adjusted number of colonies in irradiated plate by the
21 adjusted number of colonies in unirradiated control. For plotting, averaged data from biological
22 replicates and was fitted with a sigmoid curve using the “[Agonist] vs. response” function in GraphPad
23 Prism software v8. Statistically significant differences in background integration frequency between
24 wild type and mutant lines were determined by one way ANOVA with Dunnett’s multiple comparisons
25 test and are indicated with asterisks (* $p \leq 0.05$, ** $p \leq 0.01$, *** $p \leq 0.001$, **** $p \leq 0.0001$). In the
26 experiments involving kinase inhibitors, the stock solutions of chemicals (Ku-55933 10 mM in DMSO,
27 VE-821 10 mM in DMSO, caffeine 40 mM in ES media, UCN-01 100 μ M in DMSO, Wortmannin 1 mM
28 in DMSO) were added to the media after seeding; 6 hr later media was collected and replaced with
29 fresh media; collected media was centrifuged to pellet the cells, which were returned to the dish.
30 For FACS-based S-RI assays cells were electroporated with pEGFP-N1 or pAZ095, plated into 6 cm
31 dishes at 3-6 x 10⁵ per dish and irradiated. One or two days later the percentage of GFP-positive cells
32 was determined (transient transfection efficiency). Upon reaching confluence cells were replated at
33 1:5-1:10 dilution into 6-well plates; this was repeated until 10-14 days after transfection at which
34 point the percentage of GFP-positive cells (RI frequency) was measured.

1 Immunoblotting

2 Immunoblotting was performed following standard protocol by wet transfer to nitrocellulose or PVDF
3 membrane, blocking and antibody dilution solution contained 5% dry skim milk, 0.05% Tween 20 in
4 PBS. Secondary antibodies were either HRP-conjugated detected with ECL (GE), or fluorescent (Sigma,
5 anti-mouse CF680 SAB4600199, anti-rabbit CF770 SAB4600215) detected with Odyssey CLx scanner
6 (LiCOR). Primary antibodies: 53BP1 (Novus Biologicals, NB100-304), H2AX (Cell Signaling, #2595),
7 γ H2AX (pS139, Millipore JBW301), MDC1 ("exon8", Abcam, ab11171 and P2B11, Millipore, 05-1572),
8 MCPH1 (Cell Signaling, #4120), Cyclin A (Santa Cruz, C-19), PARP-1 (ENZO, C-2-10).

9 Virus production

10 For rAAV production a confluent 10 cm dish of HEK293T cells was trypsinized and seeded at 1:2
11 dilution into a fresh 10 cm dish with 17 ml growth media. Calcium phosphate transfection was
12 performed by mixing 10 μ g each of the packaging (pHelper and pAAV-RC2) and 10 μ g rAAV genome
13 encoding GFP (pAAV-GFP) plasmids, 100 μ l 2.5 M CaCl_2 , deionised water to 1 ml; then 1 ml 2xHBS
14 (16.4 g/l NaCl, 11.9 g/l HEPES, 0.21 g/l Na_2HPO_4 ; pH7.1 with NaOH) was added while bubbling air
15 through the solution. The transfection mix was added dropwise to the cells. Media was changed next
16 day and 10^6 HeLa cells were seeded for infection. Two days after transfection HEK293T cells were
17 washed and dispersed with PBS containing 10 mM EDTA, pelleted, re-suspended in 1 ml media, frozen
18 on dry ice/ethanol bath and thawed at 37 °C; the freeze-thaw cycle was performed the total of four
19 times. Lysate was centrifuged at 10,000 rcf for 10 min. Half of the lysate was used to infect the HeLa
20 cells. One day after infection HeLa cells were trypsinized and counted, divided over 10-15 10-cm
21 dishes, which were irradiated with various doses. An aliquot was analyzed by FACS to determine the
22 transduction efficiency. On days 5-8 cells were checked and passaged if confluent. FACS analysis to
23 determine the fraction of cells still expressing GFP was performed on days 8 to 13.

24 D64V mutation inactivating the integrase was introduced into lentiviral packaging plasmid
25 pMDLg/pRRE by replacing the AgeI-AflIII fragment with two overlapping PCR products, with mutation
26 in the overlap, using Gibson assembly (pAZ139). HEK293T cells were transfected by calcium
27 phosphate precipitation as described above with the third generation lentiviral packaging constructs
28 pRSV-Rev, pMDLg/pRRE D64V (pAZ139),⁸¹ and the plasmid encoding lentiviral genome with PGK-
29 puroR (pLKO.1) alone or additionally with CMV-TurboGFP (SHC003, Sigma). Virus containing media
30 was collected on days 2 and 3 after transfection, diluted 1:2 with the appropriate growth media and
31 used to infect IB10 or HeLa cells (2x 10 cm-dishes). One day after the second infection the target cells
32 were collected, pooled, distributed over three 145-mm dishes and irradiated with 0, 100, 400 mGy.
33 Puromycin selection was started one day after irradiation.

34

1 Acknowledgements

2 We a thank Andre Nussenzweig and Frederick W. Alt for *H2ax*^{-/-} lines, Francis Stewart, Hein te Riele,
3 Titia Sixma and Alan Bradley for providing plasmid constructs, Gaëlle Legube for providing the AID-
4 AsiSI-ER cell line, Yanto Ridwan for help with the micro-CT irradiations. This research was funded by
5 the Gravitation program CancerGenomiCs.nl from the Netherlands Organization for Scientific
6 Research (NWO) and is part of the Oncode Institute, which is partly financed by the Dutch Cancer
7 Society.

8 Author contributions

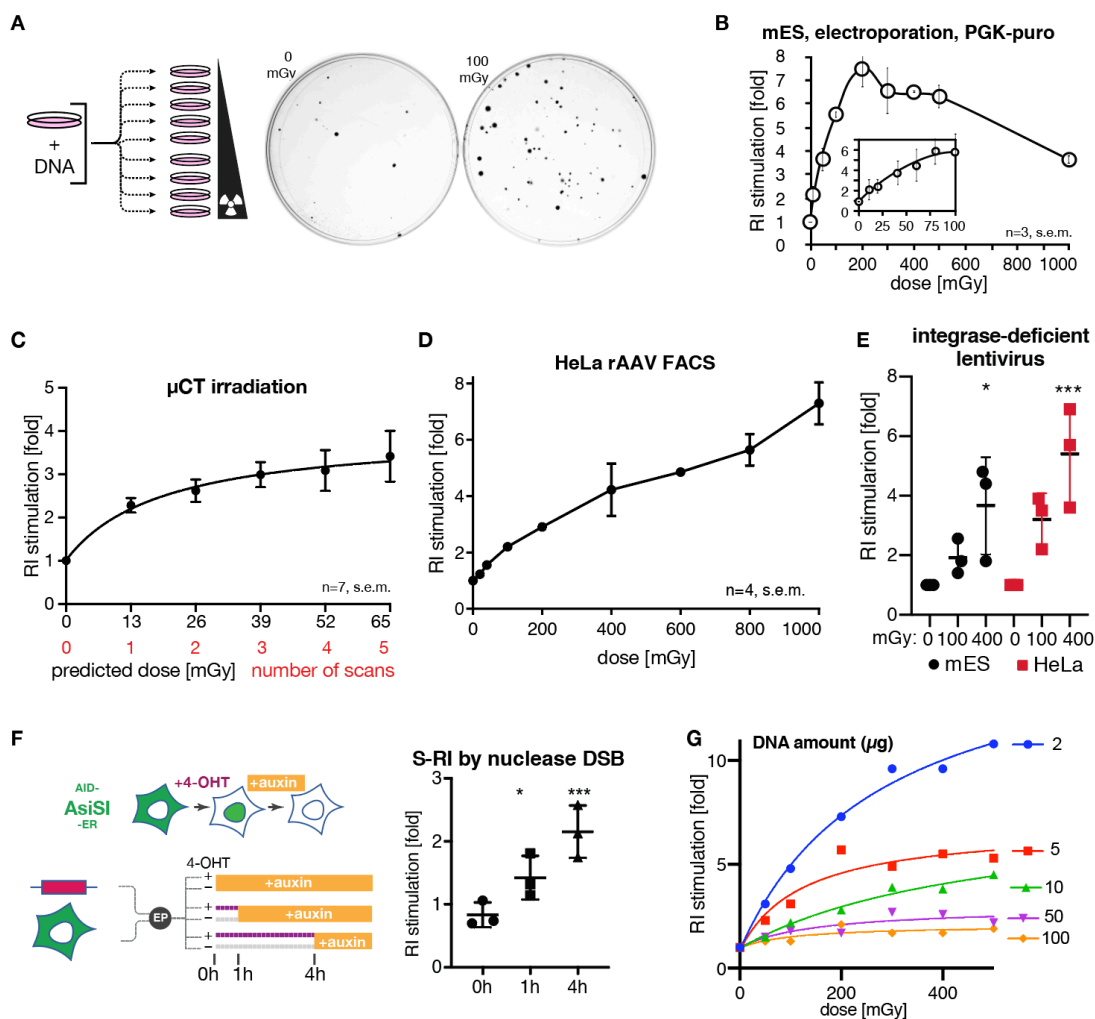
9 AZ and RK conceived and guided the study. AZ, MS, IB performed the experiments. AZ, MT, DvG, JE,
10 RK supervised various parts of the study and participated in the interpretation of the results. AZ and
11 RK wrote the manuscript, with contributions from other authors. All authors read and approved the
12 manuscript.

13 Competing interests

14 Authors declare no competing interests.

15

1 **Figures**



3 **Figure 1 RI is strongly stimulated by low doses of ionizing radiation** (A) Scheme of the typical S-R-I assay, in which antibiotic-resistant colony formation is used as an end point. Cells are transfected with linear or circular plasmid DNA, divided over a series of dishes and irradiated with different doses. After 6-8 days of antibiotic selection, plates are stained and colonies counted. Representative examples of an unirradiated plate and a plate irradiated with 100 mGy are shown at the right. (B) Mouse ES cells were electroporated with linearized plasmid with puromycin resistance gene. Colony numbers were normalized to unirradiated control to give the fold increase in RI efficiency, which is plotted. (C) mES cells were electroporated with linear or circular pLPL plasmid, divided evenly into 6 vessels, and subjected to the indicated number of low resolution micro-CT scans in a Quantum FX instrument. Indicated doses are based on manufacturer's specification. n=7, error bars show s.e.m. (D) S-R-I in HeLa cells infected with rAAV2-GFP and irradiated with the indicated doses one day later. Cells were maintained without selection, passaged when they reached confluency and sampled by FACS up to day 14. Representative FACS plots are shown in [Fig S1C]. The fraction of GFP positive cells in irradiated cultures normalized to unirradiated control is plotted. (E) S-R-I in mES and HeLa cells infected with IDLV carrying puromycin-resistance gene and irradiated with the indicated doses. Ratio of colony numbers in irradiated to unirradiated plates determined in each experiment is plotted. Statistical significance indicated by asterisks was determined by ANOVA: * p \leq 0.05, *** p \leq 0.001. (F) S-R-I by nuclease DSB. AID-AsiSI-ER U2OS cells containing a stably integrated coding sequence for AsiSI nuclease tagged with auxin-inducible degenon (AID) and estrogen receptor (ER) domain that triggers re-localization from cytoplasm to the nucleus upon addition of tamoxifen (4-OHT). Cells were electroporated with linearized plasmid PGK-puro DNA and seeded immediately into dishes containing either 0 or 300 nM 4-OHT. Auxin was added at the indicated time points to induce AsiSI degradation. The ratio of puromycin resistant colony numbers formed in plates that contained 300 nM 4-OHT was divided by the number of colonies in 0 nM plates. Statistical significance indicated by asterisks was determined by ANOVA: * p \leq 0.05, *** p \leq 0.001. (G) Effect of the amount of transfected DNA on S-R-I efficiency determined using colony-formation S-R-I assay.

23

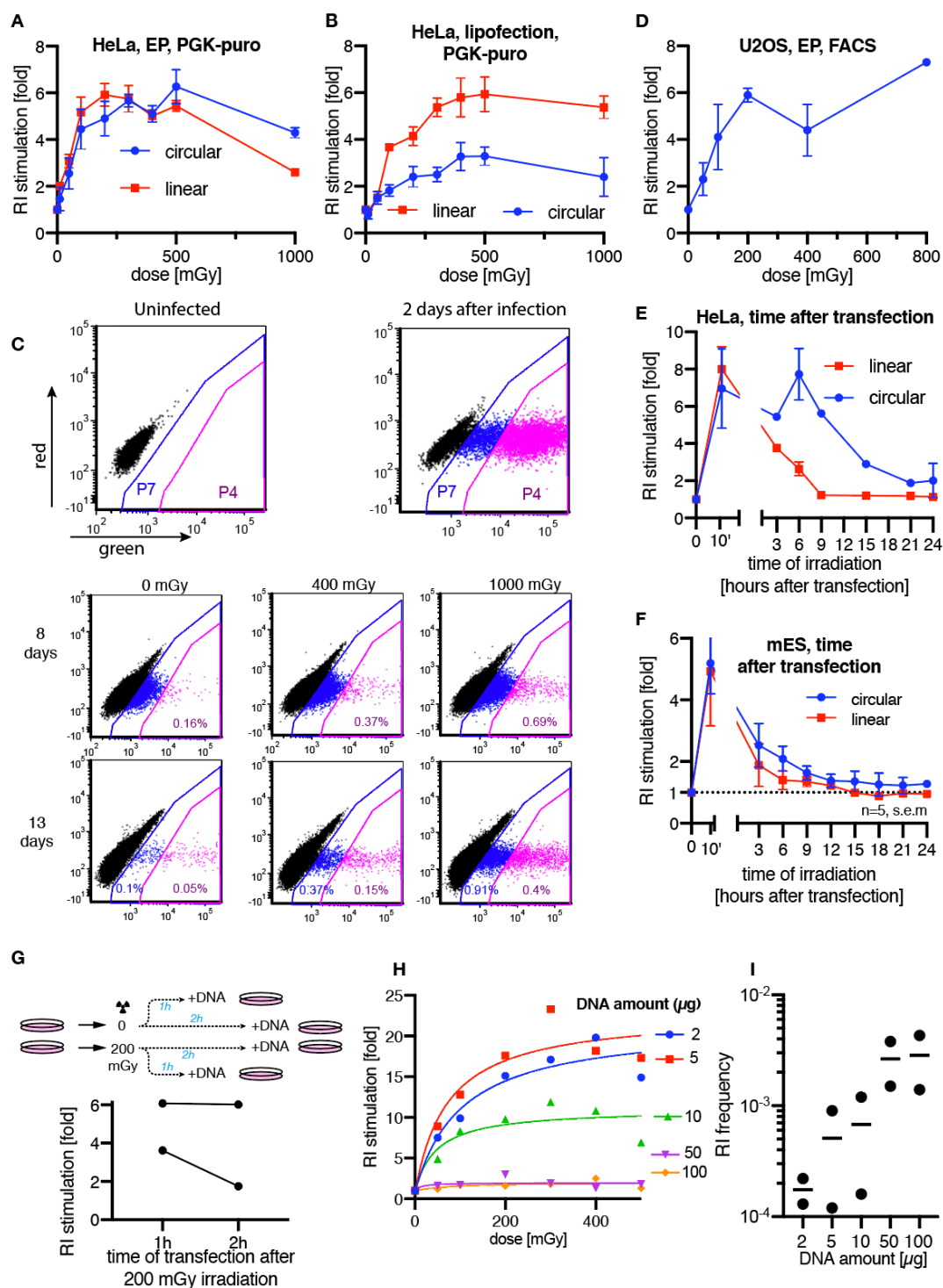
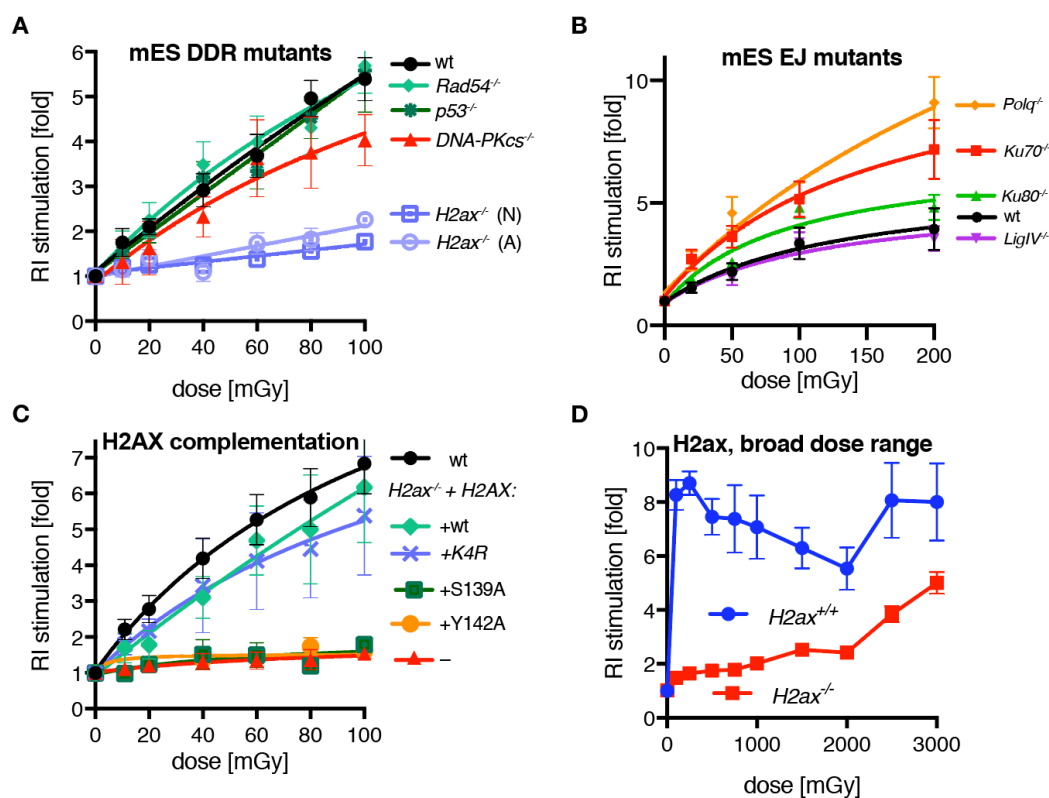


Figure S1 (related to Figure 1) (A) S-Ri in HeLa cells transfected by electroporation with linear or circular plasmid DNA carrying puromycin resistance gene under a PGK promoter. (B) S-Ri in HeLa cells transfected by lipofection. (C) Representative FACS plots from the rAAV S-Ri experiments shown in [Fig 1D]. HeLa cells infected with rAAV2-GFP virus and analyzed at different time points after infection. Gates P4 and P7 were used to calculate the fraction of high GFP-positive and all GFP-positive cells, respectively. Percentage of GFP-positive cells drops precipitously from day 2 to day 8. At 8 days post infection the broader gate (P7) still contains cells that express GFP from transient infection, while the more stringent gate contains cells stably expressing GFP. (D) FACS-based S-Ri assay performed with U2OS cells electroporated with the GFP-encoding plasmid DNA. (E) Stimulation of RI in HeLa cells electroporated with circular or linear plasmid DNA and irradiated with 0.2 Gy at different time points after electroporation. (F) Stimulation of RI in mES cells electroporated with circular or linear plasmid DNA and irradiated with 1 Gy at different time points after electroporation. Colony numbers were adjusted for reduced viability due to irradiation, and normalized to unirradiated control. (G) RI stimulation by irradiation of mES cells before transfection with linearized PGK-puro plasmid. Results of two independent experiments are plotted. (H) Repeat of the experiment shown in [Fig 1G]. (I) Background RI frequency (number of puromycin-resistant colonies per viable cell plated) from the experiments reported in [Fig 1G, S1H].

1

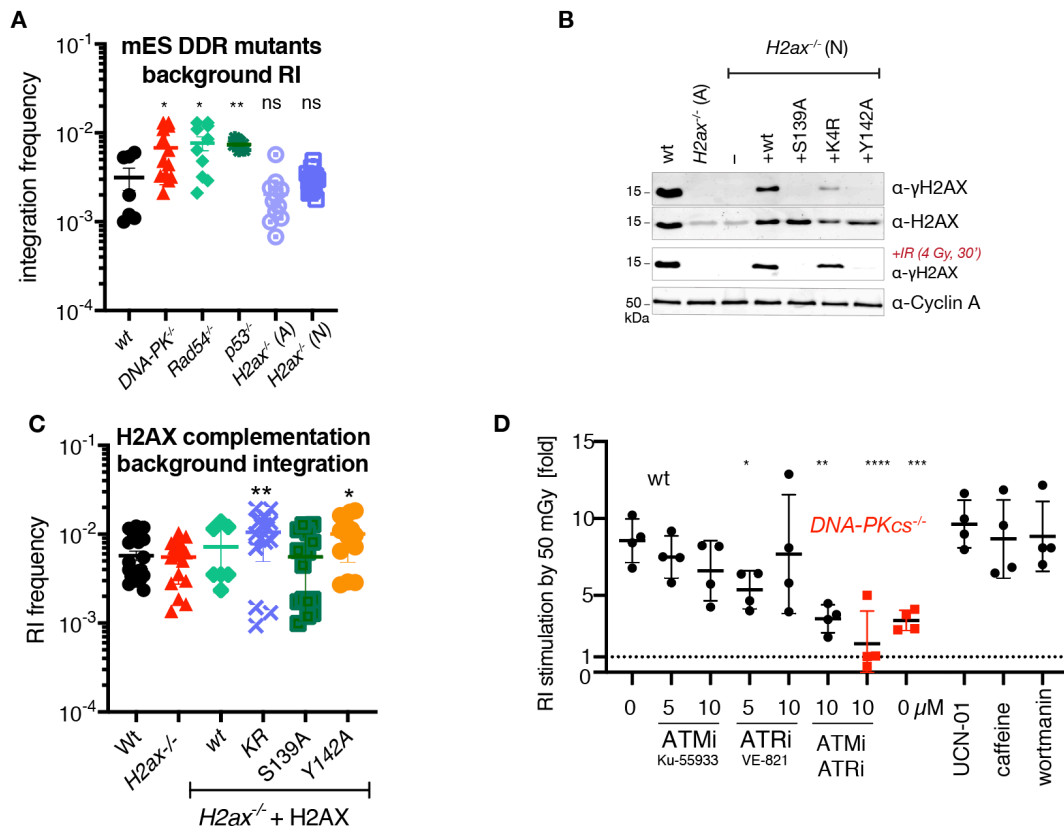


2

Figure 2 Genetic dependencies of the IR-stimulated random integration (A) Colony-based S-RI assay performed with mES cells deficient for key DSB repair and DNA damage response (DDR) proteins. The numbers of colonies obtained after puromycin selection were normalized to the unirradiated control. Means from at least 3 independent experiments, fitted with sigmoid curve, are plotted; error bars show s.e.m. (B) mES lines deficient for end joining proteins were assayed as in panel (A). (C) *H2ax*^{-/-} (N) cells were complemented with versions of H2AX containing mutations in the residues involved in key post-translational modifications during the DNA damage response. A single copy of the respective *H2AX* genes was inserted in to the *Rosa26* locus. n=3, s.e.m. K4R designates a mutant in which four lysines subject to ubiquitination were replaced with arginines. (D) S-RI response to broad irradiation dose range of *H2ax*^{-/-} and wild-type mES cells was measured in a colony-based assay. Each point represents means of at least six biological replicas, error bars indicated s.e.m. Both (N) and (A) *H2ax*^{-/-} lines were used.

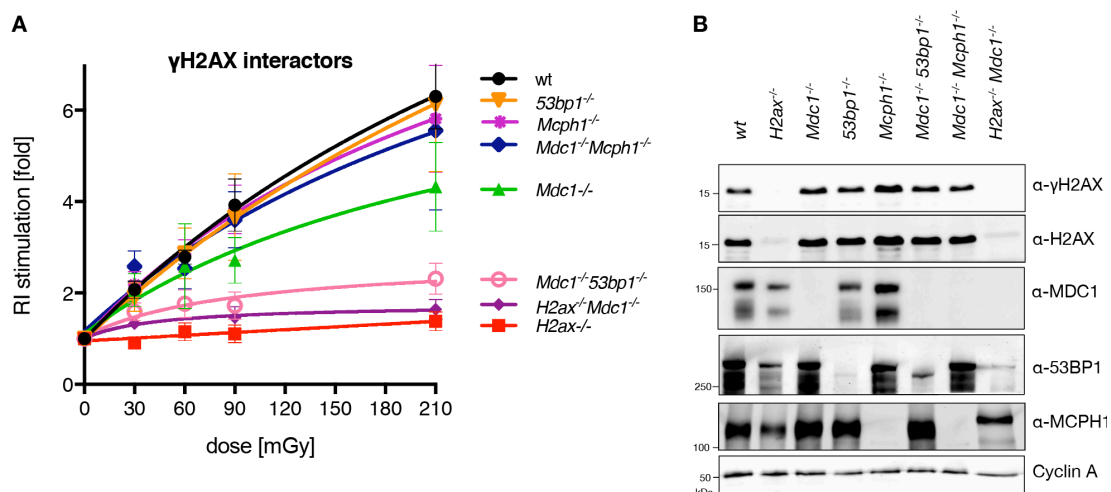
12

1



2

3 **Figure S2 Genetic dependencies of stimulated random integration (related to Figure 2)** (A) Background RI in the mutant cell
4 lines used in S-RI assay from [Fig 2A]. Individual values from biological replicas are plotted, with bars indicating means \pm s.e.m.
5 Statistical significance was determined using one-way ANOVA with Dunnett's multiple comparison test. (B) Immunoblot of *H2ax*
6 ^{-/-} and complemented lines. Total cell lysates from wild-type, *H2ax*^{-/-} (A) and (N) lines, and *H2ax*^{-/-} (N) line complemented with
7 various H2AX mutants, were immunoblotted with the indicated antibodies. To test γ H2AX induction cells were irradiated with 4
8 Gy and lysed 30 minutes after. (C) Background RI measured as in panel (A) in cells used in [Fig 2C]. (D) Effect of DNA damage
9 response kinase inhibitors on S-RI in wild-type (black circles) and *DNA-PKcs*^{-/-} (red squares) mES cells. Cells were electroporated
10 with linearized plasmid, seeded into dishes containing the indicated concentrations of the inhibitors and irradiated with 50 mGy.
11 The chemicals were removed 6 hours later. Data from four independent experiments is plotted.



1

2 **Figure 3 S-R1 dependence on γ H2AX-interacting proteins** (A) Colony formation based S-R1 assay was performed on mES cells in
 3 which genes encoding the three known γ H2AX-interacting proteins were inactivated by CRISPR/Cas9-assisted gene targeting. (B)
 4 Immunoblot on the whole cell lysates from the knock-out lines used in panel (A), confirming the loss of protein expression from
 5 targeted genes.

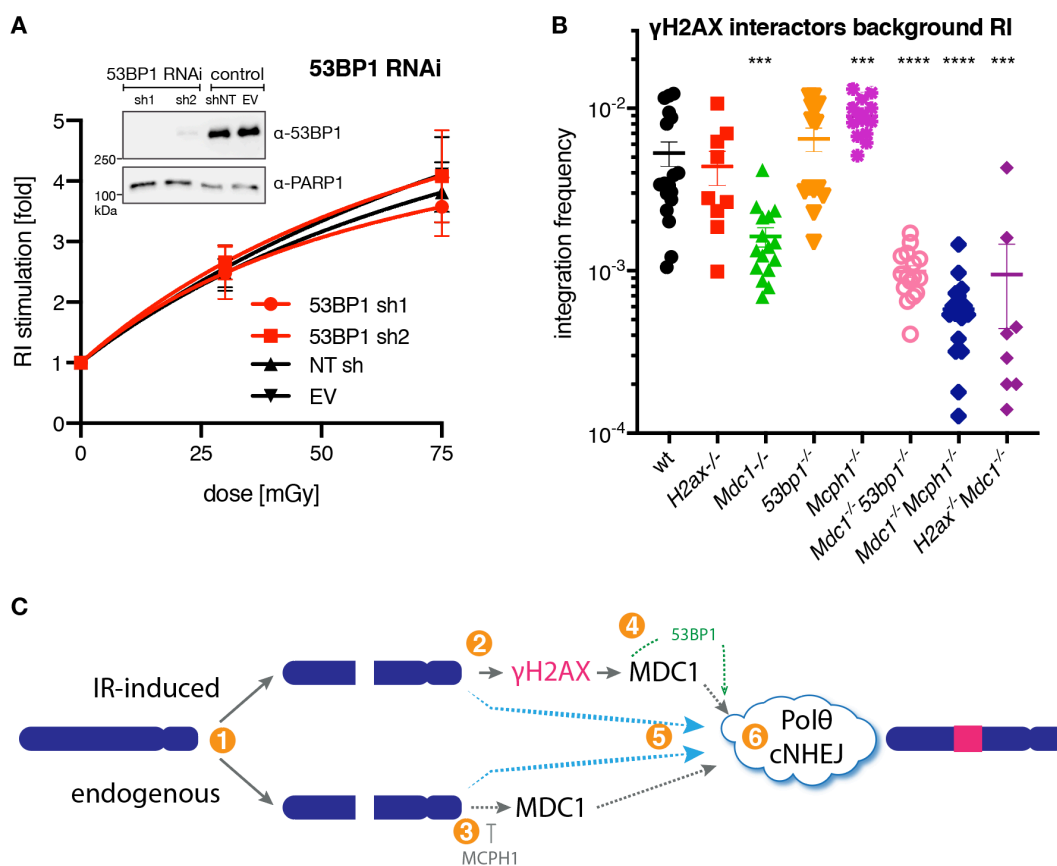


Figure S3 (related to Figure 3) (A) 53BP1 knock-down does not affect S-RI efficiency. Means of four independent puromycin-resistant colony formation S-RI assays (two with linearized, two with circular plasmid DNA) are plotted. Immunoblot on total cell lysates with the indicated antibodies confirming the efficiency of knock-down is shown as an inset. (B) Background RI efficiency in mES cell lines deficient for γ H2AX interacting proteins. Data is plotted as in [Fig S2A]. (C) A model of RI and S-RI, based on the supposition that the initial stages of the two processes are mechanistically distinct 1, to account for the observation that S-RI is γ H2AX-dependent 2, while RI is not 3; MCPH1 competes with MDC1 for γ H2AX binding, and its removal results in elevated RI 3. MDC1 contributes to both RI and S-RI 4, and 53BP1 can provide a backup mechanism for S-RI in the absence of MDC1, but does not contribute to the RI process 4. Since neither RI nor S-RI are completely abolished by the deletion of the proteins listed in the scheme, alternative pathways must exist 5. The final ligation steps are mediated by Pol θ or cNHEJ, as we previously showed that all integration events in ES cells are abolished when both these end joining mechanisms are inactivated, however the relative contribution of Pol θ and cNHEJ to RI and S-RI may be different.

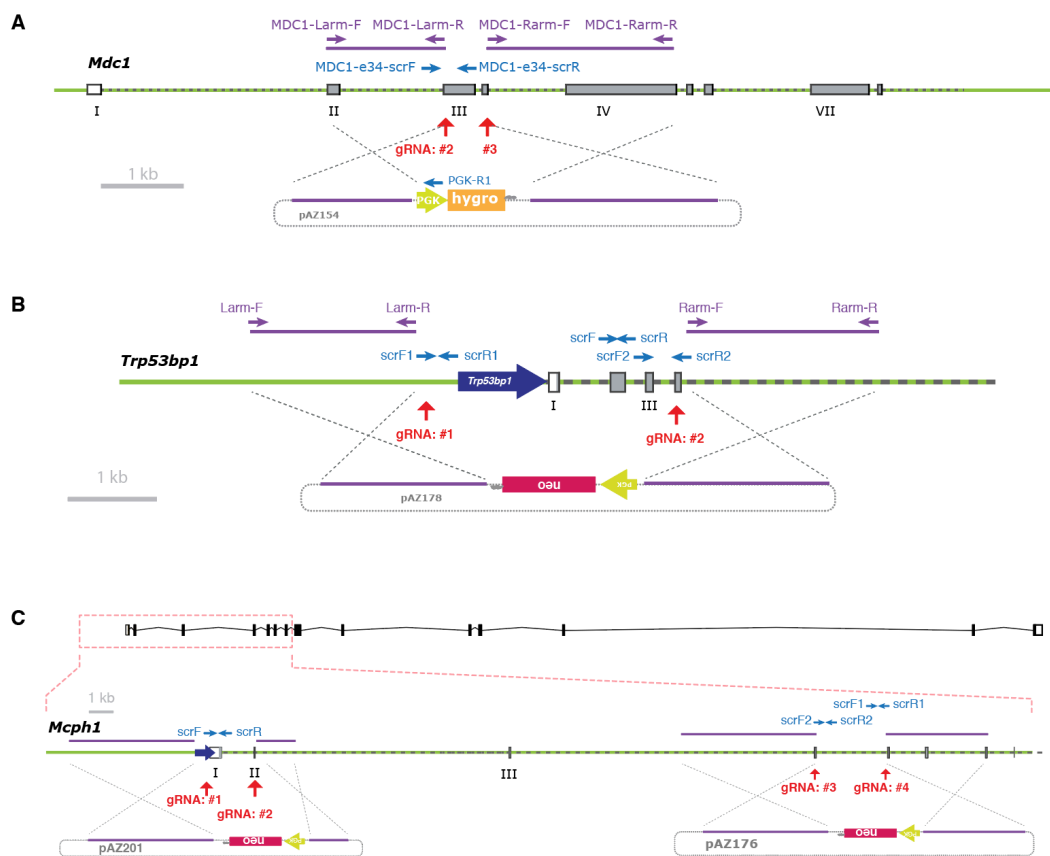


Figure S4 Generation of knock-out mES lines by CRISPR/Cas9-assisted gene targeting Schemes of mouse loci (A) *Mdc1*, (B) *53bp1* and (C) *Mcph1* and of the corresponding gene targeting construct are shown. CRISPR/Cas9 cut sites (gRNA recognition sequences) are indicated with red arrows. Homology arms and PCR primers used to amplify them from genomic DNA for cloning into the gene targeting construct are shown as violet bars and arrows, respectively. Locations of the PCR primers used to screen for homozygously targeted clones are shown as blue arrows. Endogenous and synthetic promoters are shown as thick arrows. Exons and antibiotic resistance genes are shown as bars.

1
2
3
4
5
6
7
8

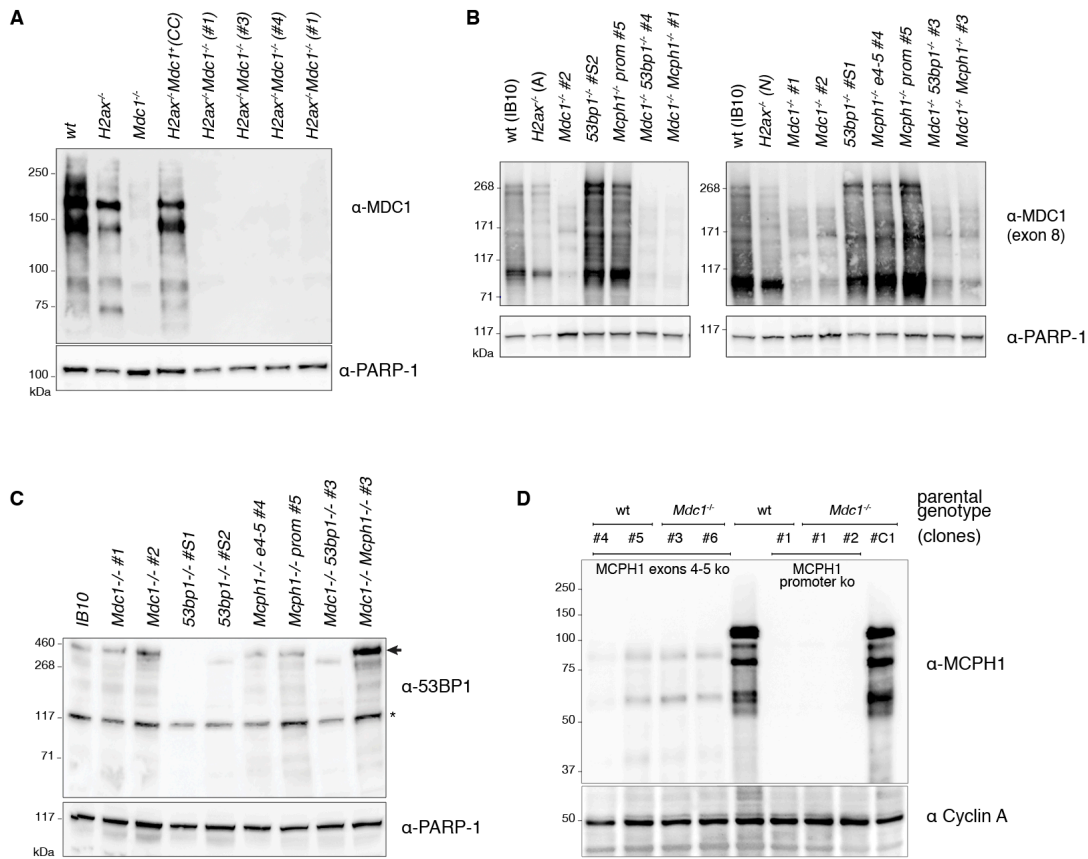


Figure S5 Immunoblots confirming the loss of protein expression from targeted genes Total cell extracts from the mES cell lines with indicated genotypes were fractionated by SDS-PAGE and immunoblotted with the indicated antibodies: **(A)** anti-MDC1 monoclonal and **(B)** polyclonal raised against the region encoded by exon 8, **(C)** anti-53BP1 and **(D)** anti-MCPH1. Membranes were re-probed with anti-PARP-1 antibody to assess relative loading. For each genotype at least two independent clones used in the experiments were tested. Clones that were derived from the CRISPR/Cas9-assisted gene targeting procedure but retained the wild-type allele (as determined by PCR genotyping) were used as controls in some experiments; these are indicated with letter C. Asterisk indicates non-specific band.

1

2 References

3

4

1. Uren, A. G., Kool, J., Berns, A. & van Lohuizen, M. Retroviral insertional mutagenesis: past, present and future. *Oncogene* **24**, 7656–7672 (2005).
2. Chen, Y., Williams, V., Filippova, M., Filippov, V. & Duerksen-Hughes, P. Viral Carcinogenesis: Factors Inducing DNA Damage and Virus Integration. *Cancers* **6**, 2155–2186 (2014).
3. Capecchi, M. R. Altering the genome by homologous recombination. *Science* **244**, 1288–1292 (1989).
4. Nabetani, A. & Ishikawa, F. Unusual telomeric DNAs in human telomerase-negative immortalized cells. *Mol Cell Biol* **29**, 703–713 (2009).
5. Schnepf, B. C., Jensen, R. L., Chen, C.-L., Johnson, P. R. & Clark, K. R. Characterization of adeno-associated virus genomes isolated from human tissues. *J. Virol.* **79**, 14793–14803 (2005).
6. Bergsmedh, A. *et al.* Horizontal transfer of oncogenes by uptake of apoptotic bodies. *Proc Natl Acad Sci USA* **98**, 6407–6411 (2001).
7. Shibata, Y. *et al.* Extrachromosomal microDNAs and chromosomal microdeletions in normal tissues. *Science* **336**, 82–86 (2012).
8. Würtele, H., Little, K. C. E. & Chartrand, P. Illegitimate DNA integration in mammalian cells. *Gene Ther.* **10**, 1791–1799 (2003).
9. Kamekawa, H., Kurosawa, A., Umehara, M., Toyoda, E. & Adachi, N. Endogenous Factors Causative of Spontaneous DNA Damage that Leads to Random Integration in Human Cells. *Gene Technology* **02**, 1–5 (2013).
10. Hillman, G. G. *et al.* Radiation improves intratumoral gene therapy for induction of cancer vaccine in murine prostate carcinoma. *Hum. Gene Ther.* **14**, 763–775 (2003).
11. Kiechle, M., Manivasakam, P., Eckardt-Schupp, F., Schiestl, R. H. & Friedl, A. A. Promoter-trapping in *Saccharomyces cerevisiae* by radiation-assisted fragment insertion. *Nucleic Acids Res.* **30**, e136 (2002).
12. Stevens, C. W., Puppi, M. & Cerniglia, G. J. Time-dose relationships in radiation-enhanced integration. *Int J Radiat Biol* **77**, 841–846 (2001).
13. Zeng, M., Cerniglia, G. J., Eck, S. L. & Stevens, C. W. High-efficiency stable gene transfer of adenovirus into mammalian cells using ionizing radiation. *Hum. Gene Ther.* **8**, 1025–1032 (1997).
14. Iwamoto, R., Fushimi, K., Hiraki, Y. & Namba, M. Enhancement of DNA-transfection frequency by X-rays. *Acta Med Okayama* **51**, 19–23 (1997).
15. Stevens, C. W., Zeng, M. & Cerniglia, G. J. Ionizing radiation greatly improves gene transfer efficiency in mammalian cells. *Hum. Gene Ther.* **7**, 1727–1734 (1996).
16. Alexander, I. E., Russell, D. W. & Miller, A. D. DNA-damaging agents greatly increase the transduction of nondividing cells by adeno-associated virus vectors. *J. Virol.* **68**, 8282–8287 (1994).
17. Rubin, J. S. Effect of gamma rays on efficiency of gene transfer in DNA repair-proficient and -deficient cell lines. *Somat Cell Mol Genet* **14**, 613–621 (1988).
18. Perez, C. F., Botchan, M. R. & Tobias, C. A. DNA-mediated gene transfer efficiency is enhanced by ionizing and ultraviolet irradiation of rodent cells in vitro. I. Kinetics of enhancement. *Radiat Res* **104**, 200–213 (1985).
19. Debenham, P. G. & Webb, M. B. The effect of X-rays and ultraviolet light on DNA-mediated gene transfer in mammalian cells. *Int J Radiat Biol Relat Stud Phys Chem Med* **46**, 555–568 (1984).
20. Yang, T. C. *et al.* Enhancement effects of high-energy neon particles on the viral transformation of mouse C3H10T1/2 cells in vitro. *Radiat Res* **81**, 208–223 (1980).
21. Coggin, J. H. Enhanced virus transformation of hamster embryo cells in vitro. *J. Virol.* **3**, 458–462 (1969).

52

- 1 22. Pollock, E. J. & Todaro, G. J. Radiation enhancement of SV40 transformation in 3T3 and
2 human cells. *Nature* **219**, 520–521 (1968).
- 3 23. Stoker, M. EFFECT OF X-IRRADIATION ON SUSCEPTIBILITY OF CELLS TO TRANSFORMATION BY
4 POLYOMA VIRUS. *Nature* **200**, 756–758 (1963).
- 5 24. Lin, E. C. Radiation risk from medical imaging. *Mayo Clin. Proc.* **85**, 1142–6– quiz 1146 (2010).
- 6 25. Kaeppl, C. *et al.* A largely random AAV integration profile after LPLD gene therapy. *Nat Med*
7 **19**, 889–891 (2013).
- 8 26. Miller, D. G., Petek, L. M. & Russell, D. W. Adeno-associated virus vectors integrate at
9 chromosome breakage sites. *Nat Genet* **36**, 767–773 (2004).
- 10 27. Yáñez-Muñoz, R. J. *et al.* Effective gene therapy with nonintegrating lentiviral vectors. *Nat*
11 *Med* **12**, 348–353 (2006).
- 12 28. Vargas, J., Gusella, G. L., Najfeld, V., Klotman, M. E. & Cara, A. Novel integrase-defective
13 lentiviral episomal vectors for gene transfer. *Hum. Gene Ther.* **15**, 361–372 (2004).
- 14 29. Leavitt, A. D., Robles, G., Alesandro, N. & Varmus, H. E. Human immunodeficiency virus type 1
15 integrase mutants retain in vitro integrase activity yet fail to integrate viral DNA efficiently
16 during infection. *J. Virol.* **70**, 721–728 (1996).
- 17 30. Wang, X. *et al.* Unbiased detection of off-target cleavage by CRISPR-Cas9 and TALENs using
18 integrase-defective lentiviral vectors. *Nat Biotechnol* **33**, 175–178 (2015).
- 19 31. Gabriel, R. *et al.* An unbiased genome-wide analysis of zinc-finger nuclease specificity. *Nat*
20 *Biotechnol* **29**, 816–823 (2011).
- 21 32. Aymard, F. *et al.* Transcriptionally active chromatin recruits homologous recombination at
22 DNA double-strand breaks. *Nature Structural and Molecular Biology* **21**, 366–374 (2014).
- 23 33. Essers, J. *et al.* Disruption of mouse RAD54 reduces ionizing radiation resistance and
24 homologous recombination. *Cell* **89**, 195–204 (1997).
- 25 34. Gao, Y. *et al.* A targeted DNA-PKcs-null mutation reveals DNA-PK-independent functions for
26 KU in V(D)J recombination. *Immunity* **9**, 367–376 (1998).
- 27 35. Zelensky, A. N., Schimmel, J., Kool, H., Kanaar, R. & Tijsterman, M. Inactivation of Pol θ and C-
28 NHEJ eliminates off-target integration of exogenous DNA. *Nat Commun* **8**, 66 (2017).
- 29 36. Saito, S., Maeda, R. & Adachi, N. Dual loss of human POLQ and LIG4 abolishes random
30 integration. *Nat Commun* **8**, 16112 (2017).
- 31 37. Bassing, C. H. *et al.* Increased ionizing radiation sensitivity and genomic instability in the
32 absence of histone H2AX. *Proc Natl Acad Sci USA* **99**, 8173–8178 (2002).
- 33 38. Celeste, A. *et al.* Genomic instability in mice lacking histone H2AX. *Science* **296**, 922–927
34 (2002).
- 35 39. Bassing, C. H. *et al.* Histone H2AX: a dosage-dependent suppressor of oncogenic
36 translocations and tumors. *Cell* **114**, 359–370 (2003).
- 37 40. Franco, S. *et al.* H2AX prevents DNA breaks from progressing to chromosome breaks and
38 translocations. *Mol Cell* **21**, 201–214 (2006).
- 39 41. Rogakou, E. P., Pilch, D. R., Orr, A. H., Ivanova, V. S. & Bonner, W. M. DNA double-stranded
40 breaks induce histone H2AX phosphorylation on serine 139. *Journal of Biological Chemistry*
41 **273**, 5858–5868 (1998).
- 42 42. Stewart, G. S. *et al.* The RIDDLE syndrome protein mediates a ubiquitin-dependent signaling
43 cascade at sites of DNA damage. *Cell* **136**, 420–434 (2009).
- 44 43. Mattioli, F. *et al.* RNF168 ubiquitinates K13-15 on H2A/H2AX to drive DNA damage signaling.
45 *Cell* **150**, 1182–1195 (2012).
- 46 44. Stucki, M. *et al.* MDC1 directly binds phosphorylated histone H2AX to regulate cellular
47 responses to DNA double-strand breaks. *Cell* **123**, 1213–1226 (2005).
- 48 45. Stiff, T. *et al.* ATM and DNA-PK function redundantly to phosphorylate H2AX after exposure to
49 ionizing radiation. *Cancer Res.* **64**, 2390–2396 (2004).
- 50 46. Hickson, I. *et al.* Identification and characterization of a novel and specific inhibitor of the
51 ataxia-telangiectasia mutated kinase ATM. *Cancer Res.* **64**, 9152–9159 (2004).
- 52 47. Charrier, J.-D. *et al.* Discovery of potent and selective inhibitors of ataxia telangiectasia
53 mutated and Rad3 related (ATR) protein kinase as potential anticancer agents. *J. Med. Chem.*
54 **54**, 2320–2330 (2011).
- 55 48. Sarkaria, J. N. *et al.* Inhibition of phosphoinositide 3-kinase related kinases by the
56 radiosensitizing agent wortmannin. *Cancer Res.* **58**, 4375–4382 (1998).

- 1 49. Graves, P. R. *et al.* The Chk1 protein kinase and the Cdc25C regulatory pathways are targets of
2 the anticancer agent UCN-01. *Journal of Biological Chemistry* **275**, 5600–5605 (2000).
- 3 50. Zelensky, A. N. *et al.* Caffeine suppresses homologous recombination through interference
4 with RAD51-mediated joint molecule formation. *Nucleic Acids Res.* **41**, 6475–6489 (2013).
- 5 51. Tsabar, M., Mason, J. M., Chan, Y.-L., Bishop, D. K. & Haber, J. E. Caffeine inhibits gene
6 conversion by displacing Rad51 from ssDNA. *Nucleic Acids Res.* **43**, 6902–6918 (2015).
- 7 52. Tsabar, M. *et al.* Caffeine impairs resection during DNA break repair by reducing the levels of
8 nucleases Sae2 and Dna2. *Nucleic Acids Res.* **43**, 6889–6901 (2015).
- 9 53. Kleiner, R. E., Verma, P., Molloy, K. R., Chait, B. T. & Kapoor, T. M. Chemical proteomics
10 reveals a γ H2AX-53BP1 interaction in the DNA damage response. *Nat Chem Biol* **11**, 807–814
11 (2015).
- 12 54. Wood, J. L., Singh, N., Mer, G. & Chen, J. MCPH1 functions in an H2AX-dependent but MDC1-
13 independent pathway in response to DNA damage. *Journal of Biological Chemistry* **282**,
14 35416–35423 (2007).
- 15 55. Scully, R. & Xie, A. Double strand break repair functions of histone H2AX. *Mutat Res* **750**, 5–14
16 (2013).
- 17 56. Chen, W.-T. *et al.* Systematic identification of functional residues in mammalian histone H2AX.
18 *Mol Cell Biol* **33**, 111–126 (2013).
- 19 57. Revet, I. *et al.* Functional relevance of the histone gammaH2Ax in the response to DNA
20 damaging agents. *Proc. Natl. Acad. Sci. U.S.A.* **108**, 8663–8667 (2011).
- 21 58. Sonoda, E. *et al.* Collaborative roles of gammaH2AX and the Rad51 paralog Xrcc3 in
22 homologous recombinational repair. *DNA Repair (Amst.)* **6**, 280–292 (2007).
- 23 59. Celeste, A. *et al.* Histone H2AX phosphorylation is dispensable for the initial recognition of
24 DNA breaks. *Nat. Cell Biol.* **5**, 675–679 (2003).
- 25 60. Xie, A. *et al.* Control of sister chromatid recombination by histone H2AX. *Mol Cell* **16**, 1017–
26 1025 (2004).
- 27 61. Xie, A., Odate, S., Chandramouly, G. & Scully, R. H2AX post-translational modifications in the
28 ionizing radiation response and homologous recombination. *Cell Cycle* **9**, 3602–3610 (2010).
- 29 62. Fernandez-Capetillo, O. *et al.* DNA damage-induced G2-M checkpoint activation by histone
30 H2AX and 53BP1. *Nat. Cell Biol.* **4**, 993–997 (2002).
- 31 63. Xie, A., Kwok, A. & Scully, R. Role of mammalian Mre11 in classical and alternative
32 nonhomologous end joining. *Nature Structural and Molecular Biology* **16**, 814–818 (2009).
- 33 64. Bañuelos, C. A. *et al.* Mouse but not human embryonic stem cells are deficient in rejoining of
34 ionizing radiation-induced DNA double-strand breaks. *DNA Repair (Amst.)* **7**, 1471–1483
35 (2008).
- 36 65. Panier, S. & Boulton, S. J. Double-strand break repair: 53BP1 comes into focus. *Nat. Rev. Mol.*
37 *Cell Biol.* **15**, 7–18 (2014).
- 38 66. Zimmermann, M. & de Lange, T. 53BP1: pro choice in DNA repair. *Trends Cell Biol* **24**, 108–117
39 (2014).
- 40 67. Bunting, S. F. *et al.* 53BP1 inhibits homologous recombination in Brca1-deficient cells by
41 blocking resection of DNA breaks. *Cell* **141**, 243–254 (2010).
- 42 68. Difilippantonio, S. *et al.* 53BP1 facilitates long-range DNA end-joining during V(D)J
43 recombination. *Nature* **456**, 529–533 (2008).
- 44 69. Dimitrova, N., Chen, Y.-C. M., Spector, D. L. & de Lange, T. 53BP1 promotes non-homologous
45 end joining of telomeres by increasing chromatin mobility. *Nature* **456**, 524–528 (2008).
- 46 70. Lou, Z. *et al.* MDC1 regulates DNA-PK autophosphorylation in response to DNA damage.
47 *Journal of Biological Chemistry* **279**, 46359–46362 (2004).
- 48 71. Stewart, G. S., Wang, B., Bignell, C. R., Taylor, A. M. R. & Elledge, S. J. MDC1 is a mediator of
49 the mammalian DNA damage checkpoint. *Nature* **421**, 961–966 (2003).
- 50 72. Minter-Dykhouse, K., Ward, I., Huen, M. S. Y., Chen, J. & Lou, Z. Distinct versus overlapping
51 functions of MDC1 and 53BP1 in DNA damage response and tumorigenesis. *J Cell Biol* **181**,
52 727–735 (2008).
- 53 73. Eliezer, Y., Argaman, L., Rhie, A., Doherty, A. J. & Goldberg, M. The direct interaction between
54 53BP1 and MDC1 is required for the recruitment of 53BP1 to sites of damage. *Journal of*
55 *Biological Chemistry* **284**, 426–435 (2009).

- 1 74. Hooper, M., Hardy, K., Handyside, A., Hunter, S. & Monk, M. HPRT-deficient (Lesch-Nyhan)
2 mouse embryos derived from germline colonization by cultured cells. *Nature* **326**, 292–295
3 (1987).
- 4 75. Ran, F. A. *et al.* Genome engineering using the CRISPR-Cas9 system. *Nat Protoc* **8**, 2281–2308
5 (2013).
- 6 76. Soriano, P. Generalized lacZ expression with the ROSA26 Cre reporter strain. *Nat Genet* **21**,
7 70–71 (1999).
- 8 77. Dannenberg, J.-H., Schuijff, L., Dekker, M., van der Valk, M. & Riele, Te, H. Tissue-specific
9 tumor suppressor activity of retinoblastoma gene homologs p107 and p130. *Genes Dev.* **18**,
10 2952–2962 (2004).
- 11 78. Li, M. Z. & Elledge, S. J. SLIC: a method for sequence- and ligation-independent cloning.
12 *Methods Mol Biol* **852**, 51–59 (2012).
- 13 79. Gibson, D. G. *et al.* Enzymatic assembly of DNA molecules up to several hundred kilobases.
14 *Nat Meth* **6**, 343–345 (2009).
- 15 80. Fu, J., Anastassiadis, K. & Stewart, A. F. A recombineering pipeline to make conditional
16 targeting constructs. *Meth Enzymol* **477**, 125–144 (2010).
- 17 81. Dull, T. *et al.* A third-generation lentivirus vector with a conditional packaging system. *J. Virol.*
18 **72**, 8463–8471 (1998).
- 19